Continuous or discrete: Tuning the energy level alignment of organic layers with alkali dopants

Thomas Ules, Daniel Lüftner, Eva Maria Reinisch, Georg Koller, Peter Puschnig, and Michael G. Ramsey*
University of Graz, Institute of Physics, NAWI Graz, Universitätsplatz 5, 8010 Graz, Austria
(Received 23 June 2016; revised manuscript received 2 September 2016; published 7 November 2016)

This paper investigates the effects of cesium (Cs) deposited on pentacene (5A) and sexiphenyl (6P) monolayers on the Ag(110) substrate. The process of doping and the energy level alignment are studied quantitatively and contrasted. While ultimately for both molecules lowest unoccupied molecular orbital (LUMO) filling on charge transfer upon Cs dosing is observed, the doping processes are tellingly different. In the case of 5A, hybrid molecule-substrate states and doping states coexist at lowest Cs exposures, while for 6P doping states appear only after Cs has completely decoupled the monolayer from the substrate. With the support of density functional theory calculations, this different behavior is rationalized by the local character of electrostatic potential changes induced by dopants in relation to the spatial extent of the molecules. This also has severe effects on the energy level alignment, which for most dopant/molecule systems cannot be considered continuous but discrete.

DOI: 10.1103/PhysRevB.94.205405

I. INTRODUCTION

For efficient charge injection in organic (opto-) electronic devices, proper matching of the Fermi level of the electrode to the charge transport levels of the organic semiconductor is necessary [1]. The ideal energy level alignment would be with the highest occupied molecular orbital/lowest unoccupied molecular orbital (HOMO/LUMO) located at the Fermi level being half filled by donation/acceptance of one electron to/from the electrode [2–4]. In the zeroth approximation, this necessitates that the work function of the combined electrode/molecule system equals the ionization potential/electron affinity (IP/EA) of the respective organic molecule. However, there are several factors which further influence the work function and the energy position of the frontier electronic orbitals at the interface. Firstly, on adsorption of the organic molecules, the electrode work function will change due to pushback of the electron density of the substrate surface. Secondly, additional dipoles may form at the interface due to chemical interactions between the organic material and the substrate [1,5]. Furthermore, the electronic energy levels are affected by polarization, hybridization, and possible geometric distortion on adsorption [6,7]. For all these reasons, the energy level alignment of the frontier electronic orbitals at an organic/metal interface is difficult to predict.

There has been growing interest in tuning the energy level alignment by incorporating donors or acceptors [3,8–11]. However, these studies are often difficult to interpret due to complex growth morphologies. In this paper, the alkali metal Cs will be applied as it provides an excellent model donor system [12], particularly as its dosing is very controllable and allows for a continuous change of a metal's work function over a large range (∼3 eV) [13–15]. The question arises whether this will also allow for a continuous tuning of the organic level alignment. To address this issue, a joint angle-resolved ultraviolet photoelectron spectroscopy (ARUPS) and density functional theory (DFT) study of the Cs doping process of a pentacene (5A) and sexiphenyl (6P) monolayer on the Ag(110) substrate will be presented. These molecules are not only prominent representatives of device relevant organic molecules; they are also well suited for highlighting the importance of the local nature of surface potential modifications on the energy level alignment and doping behavior due to their different sizes and EAs.

The energy level alignment of the occupied frontier orbitals is directly accessible by ultraviolet photoemission spectroscopy (UPS) [1,5]. However, care must be taken when interpreting UPS spectra and assigning emissions to particular orbitals as the photoemission angular intensity distribution is generally highly structured and thus very dependent on the experimental geometry and the molecular orientations. This is particularly true for the device relevant oligomers as they have a high propensity to crystallize and form ordered structures with preferred orientations of the molecules [16–19]. Recently, with the development of photoemission tomography, it has been shown that the angular photoemission distribution can be understood in simple terms and predicted [20]. This makes it not only possible to definitively assign emissions to particular orbitals [21,22]; it also allows the molecular geometries to be ascertained [12,23] and even to distinguish emissions from the same molecule with different adsorption geometries [24–26].

II. EXPERIMENTAL DETAILS

All films were grown and measured *in situ* in ultrahigh vacuum (UHV). The Ag(110) substrate surface was prepared by cleaning the crystal by repeated cycles of Ar+ ion bombardment and annealing at 800 K. The 5A (6P) molecules (from Fluka) were deposited *in situ* from a thoroughly degassed evaporator such that the pressure in the system remained in the 10^{-10} mbar range during film growth. Nominal growth rates of $2-5\,\text{Å}\,\text{min}^{-1}$, as monitored by a quartz microbalance assuming a density of $1.33\,\text{gcm}^{-3}$(5A) and $1.102\,\text{gcm}^{-3}$(6P), were used. Pentacene and 6P films were grown and measured at room temperature (300 K). After deposition of 3.5 Å of 5A, the resulting monolayer low energy electron diffraction (LEED) pattern is $\begin{pmatrix} 3 & -1 \\ 1 & 4 \end{pmatrix}$. This results in a coverage of one 5A molecule per 13 Ag surface atoms ($\Theta_{5A} = 0.077$) [27]. In the

*michael.ramsey@uni-graz.at

case of the larger 6P, one molecule covers 17 Ag atoms in the monolayer ($\Theta_{6P} = 0.059$). For doping, Cs was deposited using alkali-metal getter sources from SAES Getters. The Cs exposure was calibrated via the work function reduction on the Ag(110) surface; the minimum in the Cs/Ag(110) work function of 1.6 eV is obtained at an exposure of one Cs atom per four Ag surface atoms ($\Theta_{Cs} = 0.25$), the maximum coverage on the Ag(110) surface at room temperature [14,15]. Experiments up to a Cs exposure of 0.25 were also performed in an inverted deposition order where Cs was deposited prior to 5A with similar results.

The ARUPS experiments were performed both using a VG ADES 400 spectrometer and a toroidal electron analyzer (TEA) described elsewhere [28]. Both systems had a base pressure of 10^{-10} mbar and basic sample preparation and characterization facilities. The ADES system was equipped with a noble gas discharge lamp (unpolarized helium I radiation, $h\nu = 21.2$ eV) and a goniometer-mounted electron energy analyzer, allowing ARUPS in the specular plane with an angular resolution of $\pm 1°$ and a total energy resolution of 80 meV at room temperature. A photon incidence angle of $\alpha = 60°$ was used. The TEA system was connected to the TGM-4 beamline at the synchrotron radiation facility BESSY II. A photon energy of $h\nu = 35$ eV was used. The photon incidence angle was $\alpha = 40°$, and the polarization direction was always in the specular plane. For angular emission data converted to momentum parallel to the surface (k), the formula $k = 0.51(E_{kin}[eV])^{1/2}\sin\Theta$ [Å^{-1}] was used where Θ is the electron emission angle relative to the surface normal.

III. COMPUTATIONAL DETAILS

All theoretical results are obtained within the framework of DFT using the Vienna *Ab initio* Simulation Package (VASP) code [29,30]. Calculations for 5A adsorbed on the Cs-covered Ag(110) surface have been carried out using the repeated slab approach with five layers of Ag atoms and an additional vacuum layer of 15 Å between adjacent slabs and an inserted dipole layer to avoid spurious electric field due to the asymmetric slab [31]. The generalized gradient approximation [32] is used for exchange-correlation effects, and the projector augmented-wave (PAW) approach [33] was used with a kinetic energy cutoff of 400 eV. The van der Waals interactions were taken into account according to Grimme *et al.* [34], and the geometry relaxations have been stopped after all atomic forces were below 0.01 eV/Å. Except for the bottom two silver layers, no constraints have been applied in our DFT geometry relaxations, and careful geometry relaxations with various starting points for the Cs positions and molecular tilt angles have been performed. The energetically most favorable structures for the case of heterogeneous and homogeneous

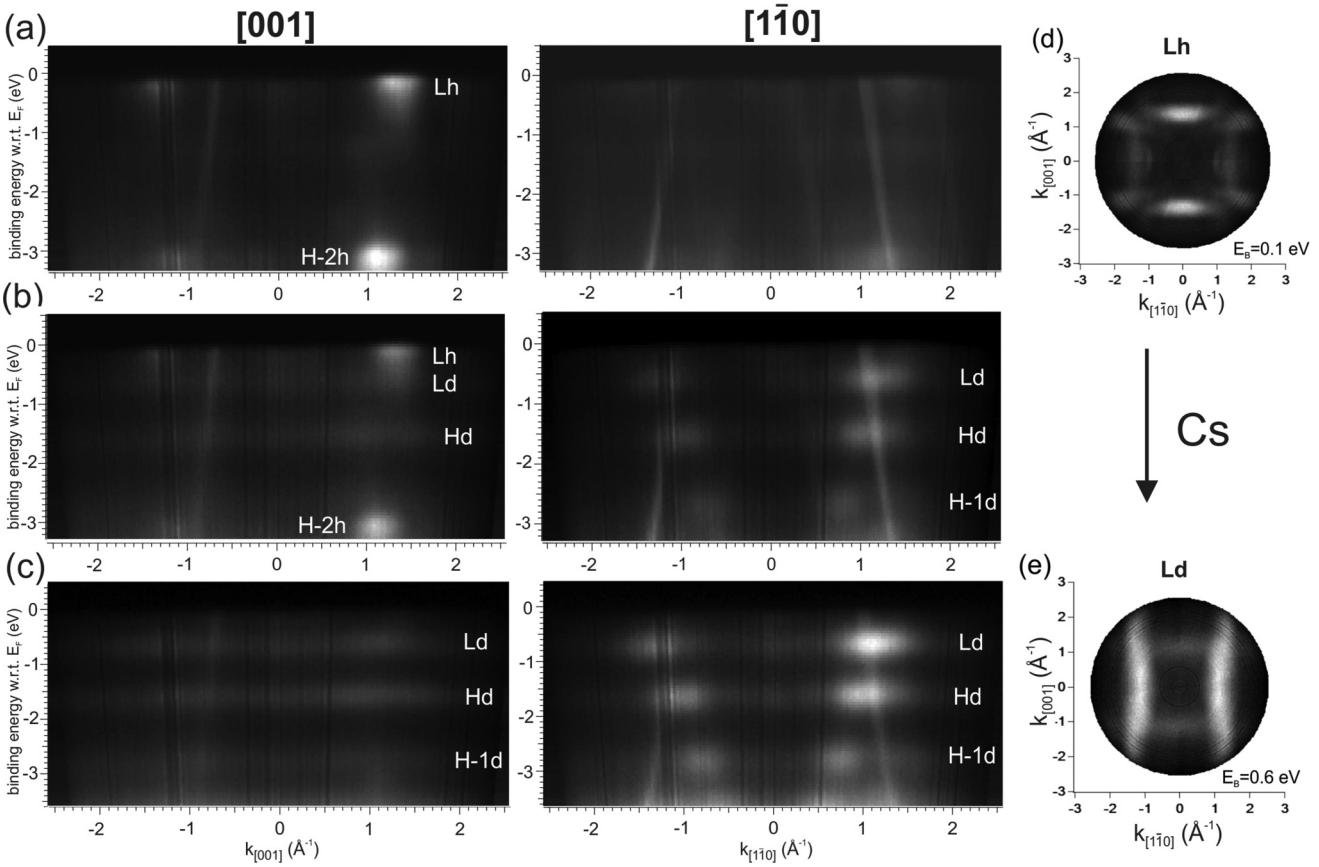

FIG. 1. Evolution of band and momentum maps of a 5A monolayer on Ag(110) upon Cs deposition. (a)–(c) Band maps in the two principal azimuths, [001] (left side) and [1$\bar{1}$0] (right side), as indicated on top of the figure. Molecular features indicated are: Lh(d), LUMO hybridized (doped); Hh(d), HOMO hybridized (doped). LUMO momentum maps of (d) hybridized and (e) doped 5A recorded at binding energies of 0.1 and 0.6 eV, respectively.

doping resulted in the model structures I and II, respectively, to be described below.

IV. RESULTS

A. 5A on Cs exposure

The photoemission tomography results shown in Fig. 1 provide an overview of the energy level alignment and the molecular orientation of a 5A/Ag monolayer upon Cs exposure. Figure 1(a) displays band maps along the [001] and [1$\bar{1}$0] azimuths of the pristine 5A monolayer without Cs. These band maps clearly demonstrate that the majority of 5A molecules are aligned along the [001] azimuth with their aromatic planes parallel to the substrate and with the LUMO half occupied upon backdonation from and hybridization with the substrate [27,35] denoted as Lh. This assignment is verified by the corresponding constant binding energy momentum map displayed in Fig. 1(d). For this molecular orientation, only LUMO and HOMO-2 are visible in the [001] azimuth, while HOMO and HOMO-1 cannot be observed in the principal azimuths [35,36]. The band map in the [1$\bar{1}$0] azimuth is dominated by the Ag *sp* band with evidence of emissions from a minority of molecules oriented along [1$\bar{1}$0].

Upon moderate Cs deposition, Fig. 1(b), a reduction in the emissions of the [001] oriented hybridized molecules can be observed, while strong molecular emissions appear in the [1$\bar{1}$0]. These will be associated with molecules that are reoriented on doping. This trend continues with Cs dosing until the emissions from the hybridized molecules (Lh and H-2h) disappear from the [001] band map and the doping-induced features reach their maximum intensity in [1$\bar{1}$0], see Fig. 1(c) [37]. In the [1$\bar{1}$0] map of Fig. 1(c), we can identify three emissions of doped 5A; the LUMO (Ld) at 0.6 eV, the HOMO (Hd) at 1.5 eV, and the HOMO-1 (H-1d) at 2.6 eV. It should be noted that, on doping, the LUMO has shifted well below E_F, suggesting full LUMO occupancy. The momentum map of Ld [Fig. 1(e)] clearly identifies it as the LUMO and demonstrates the reorientation of the long molecular axis of the molecules. The difference in appearance of this map to that of the hybridized LUMO (Lh) is a result of the molecule tilting its aromatic plane around the long molecular axis. Simulations of momentum maps with different tilt angles suggest that the molecules are tilted approximately 20°.

In order to follow the doping process in a quantitative manner, we have performed a spectral series using an experimental geometry that maximizes the doped LUMO and HOMO emissions to follow their evolution with increasing Cs exposure. To this end, we have chosen an emission angle of 35° in [1$\bar{1}$0] with He I excitation corresponding to $k_{[1\bar{1}0]} \sim 1.1$ Å^{-1}. The bottom spectrum in Fig. 2 is from the pristine 5A monolayer on Ag(110) in the [1$\bar{1}$0] azimuth. The spectrum displays the characteristics of a 5A monolayer with molecules being aligned along the [001] azimuth. The spectrum is dominated by Ag *d*-band emissions, while due to the chosen geometry, molecular emissions of hybridized flat lying 5A are weak. Upon the first Cs exposure, $\Theta_{Cs} = 0.02$, weak LUMO and HOMO emissions from doped 5A, reoriented along the Cs-induced reconstruction, appear at binding energies characteristic of doped 5A (Ld $\sim$ 0.5 eV and Hd $\sim$ 1.5 eV).

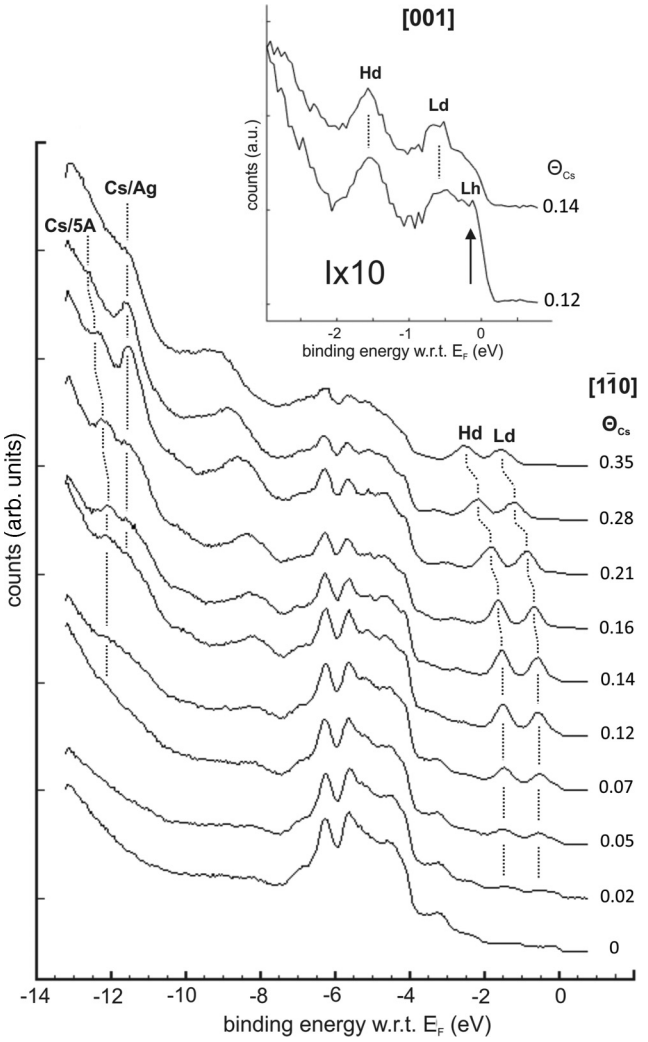

FIG. 2. Evolution of the He I ARUPS on increasing Cs deposition on a 5A monolayer on Ag(110) in the [1$\bar{1}$0] azimuth at 35° takeoff angle. The respective Cs exposures, Θ_{Cs}, are given. The LUMO and HOMO emissions of doped 5A are marked Ld and Hd. At higher binding energies, the $Cs_{5p3/2}$ emissions Cs/Ag and Cs/5A are indicated. The inset on top displays ARUPS in the [001] azimuth at 35° takeoff angle at $\Theta_{Cs} = 0.12$ and 0.14 (w.r.t., with respect to).

The work function is reduced by 0.2 eV. The trend of enhanced intensities of doped 5A features located at the characteristic binding energies of 0.5 and 1.5 eV, along with the Cs-induced work function reduction, is observed up to a Cs coverage of 0.14. Above this exposure, the work function continues to decrease, but now the emissions of doped 5A follow the change in work function and shift towards higher binding energies and broaden in energy. This second dosing regime is completed at a Cs exposure of 0.35 and a work function of 1.61 eV. Any additional Cs exposure causes no further changes to either the work function or binding energies. It should be noted that metallic Cs cannot form at room temperature due to its high vapor pressure and $\Theta_{Cs} = 0.35$ can be considered to be the Cs saturation of the molecular film and interface.

Plotting the work function (Φ) and LUMO (Ld) binding energies in Fig. 3 clearly shows two dosing regimes and indicates a change in behavior at an exposure of $\Theta_{Cs} = 0.14$.

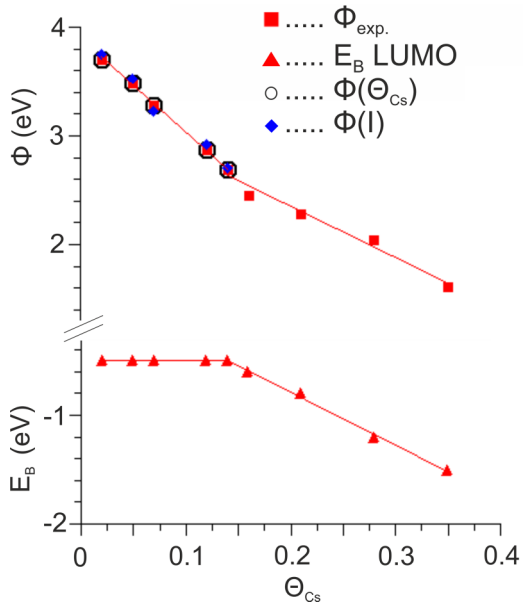

FIG. 3. Measured work functions (red squares) and LUMO binding energies referenced to Fermi level of doped 5A (red triangles) as a function of the Cs coverage (Θ_{Cs}). Additionally, work function values obtained from the percentage of doped molecules inferred from relative peak areas (blue diamonds) and from Cs coverages assuming completed monolayer doping at $\Theta_{Cs} = 0.14$ (open circles; see text for details).

To shed light on what happens at this critical exposure, spectra were taken in the [001] azimuth where the hybridized LUMO (Lh) of 90° rotated orientation can be observed. As can be seen in the inset of Fig. 2, emissions from Lh disappear between $\Theta_{Cs} = 0.12$ and 0.14, suggesting that doping of the 5A monolayer is completed, and all molecules have formed charge transfer complexes with Cs.

In addition, a LEED study has been undertaken, covering the geometric structures at the various Cs dosing stages. Up to the critical Cs exposure, a gradual decrease in the intensity of the LEED pattern of the 5A/Ag(110) monolayer is observed. Concomitantly, reflexes due to the (1 × 2) Cs reconstruction grow in intensity, while no (1 × 3) reflexes could be observed. The (1 × 2) can be seen even at the highest Cs exposure, and there is no evidence of the doped 5A overlayer having any long-range order. The LEED suggests phase separation between doped and undoped regions, but as only a single secondary cutoff is ever observed, the domains are not large. Although undoubtedly interesting in itself, a study of the phase separation and domain sizes is not within the scope of this paper.

1. First dosing regime: Doping

Completion of doping at $\Theta_{Cs} = 0.14$ is equivalent to two Cs atoms per 5A. As only two species of 5A (hybridized or doped) are observed in the doping process, it can be concluded that (a) doping requires two Cs atoms per molecule and (b) a heterogeneous surface where molecules are either bound to the Ag substrate or in a 2Cs/5A complex is favored over a homogeneous distribution with one Cs atom per molecule.

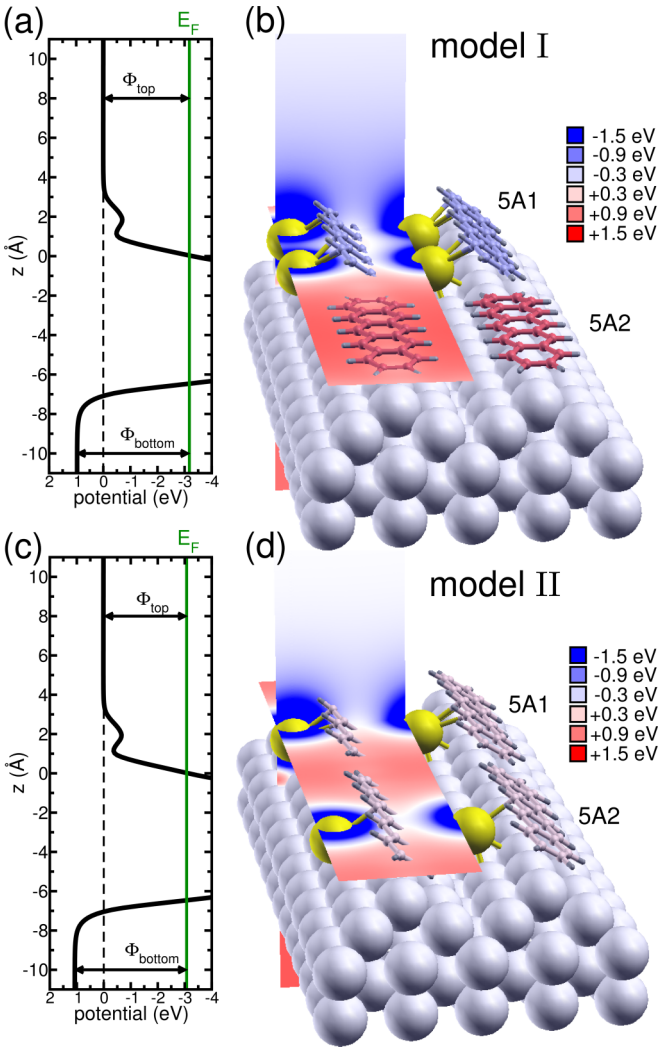

FIG. 4. Slab models of the two simulated structures together with electrostatic potential maps calculated without molecules. Molecules are displayed to illustrate their different average electrostatic potentials, expressed through their color as denoted in the text. (a) Plane-averaged electrostatic potential of model I with a heterogeneous Cs distribution in the unit cell. The resulting work functions at the top and at the bottom of the slab are indicated. (b) The corresponding slab model of the Ag(110)-(12 × 2) super cell containing two Cs atoms (yellow) and two 5A molecules. The electrostatic potential at a horizontal and a vertical cut is shown in a range from −1.5 to +1.5 eV with respect to the vacuum level on the top side of the slab. (c) and (d) are the corresponding figures for model II with a homogeneous Cs distribution in the unit cell.

This conclusion is supported by density functional calculations. We have computed the total energy difference between two model structures representing heterogeneous doping (model I) and homogeneous doping (model II). Figure 4 displays the results of these geometry-optimized structures. To make the calculations tractable, a simple (12 × 2) overlayer based on the observed Cs-induced (2 × 1) reconstruction has been employed containing two 5A molecules per unit cell. For model I, one of the molecules in the unit cell has been placed near two Cs atoms in the reconstructed Ag surface (labeled 5A1), while the other molecule (5A2) is positioned

above an undoped region of the super cell. As can be seen in panel (b), geometry relaxation leads to the 5A1 molecules tilting away from the surface plane, while the 5A2 molecules retain their planar adsorption geometry with a slight bending of the molecule, which is hardly visible in the graphical representation. For the case of a homogeneous distribution of Cs, model II, both 5A molecules (5A1 and 5A2) acquire tilted geometries with one Cs atom each located in the center of the molecule. While the tilt angle differs only by a few degrees from that of the 5A molecule 5A1 of model I, DFT reveals slightly distorted molecules as expected for a single Cs atom. We find that model I is energetically favorable over model II by 120 meV, demonstrating that the charge transfer complex with two Cs atoms per molecule, thus the heterogeneous doping scenario, is indeed preferred. It may be speculated that this energetic difference together with the high mobility of Cs adatoms at room temperature suggest that, in the first dosing regime, it is likely that two regions form on the surface. One region contains doped and tilted 5A molecules with two Cs atoms per molecule, while the other region contains flat lying undoped molecules in agreement with the experiment.

In order to understand the level alignment of the frontier orbitals of 5A, we have analyzed the electrostatic potentials based on the two model structures I and II. To this end, we have analyzed the local electrostatic potentials prior to the adsorption of the 5A molecules with the Cs atoms placed in the positions determined from the full geometry-relaxed model structure. The corresponding electrostatic potential energy landscape is shown in Figs. 4(a)–4(d) and illustrates the extent of the Cs-induced local potential relative to the size of the molecules and that the average potential is independent of the particular Cs distribution.

Panels (a) and (c) of Fig. 4 depict the plane-averaged potentials for models I and II without the 5A molecules, respectively, where the lateral averaging is done over the entire xy plane of the unit cell. The lateral mean values of both

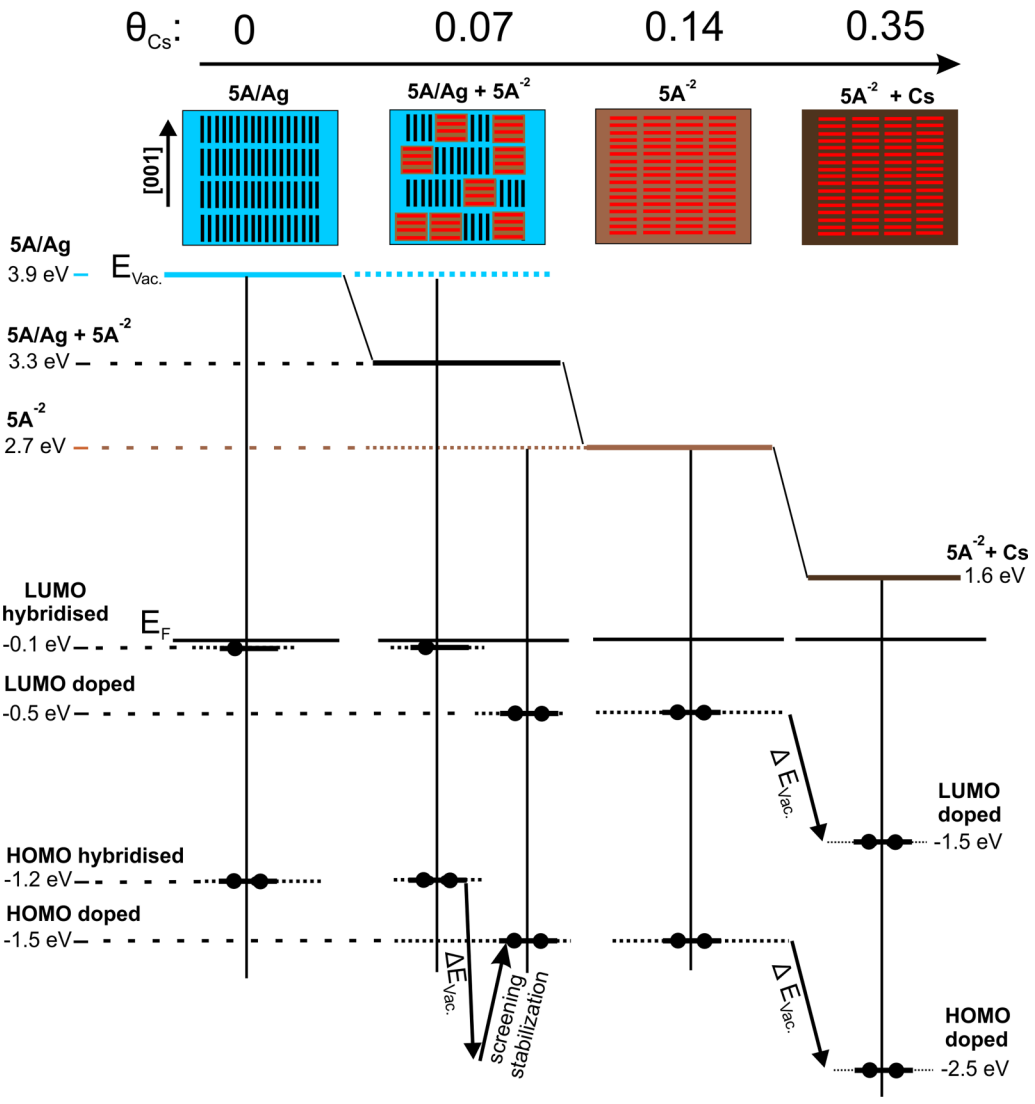

FIG. 5. Schematic of the energy level alignment for a hybridized 5A monolayer on Ag(110) on Cs doping. The first column illustrates the energy level alignment for the hybridized monolayer. The second column displays the situation for half the Cs coverage, $\Theta_{Cs} = 0.07$, of completed doping. Column 3 displays the situation at completed monolayer doping, $\Theta_{Cs} = 0.14$. Energy level alignment on additional Cs exposure, $\Theta_{Cs} = 0.35$, is illustrated in Column 4.

models give almost identical curves, suggesting the calculated average potential is independent of the particular local Cs distribution.

When measuring work functions with the secondary cutoff, one measures the effects of this average potential. However, being of finite size, the molecules will be affected by the local potential in their vicinity. When analyzing the electrostatic potential induced by the Cs atoms in a laterally resolved manner, pronounced differences between models I and II become apparent due to the extremely local effect of Cs. This can be seen from the horizontal and vertical cuts through the three-dimensional electrostatic potential landscape $\Phi(\mathbf{r})$ depicted in panels (b) and (d), respectively. In particular, we have analyzed the local electrostatic potential at the sites for the 5A1 and 5A2 molecules in the following way:

$$\bar{\Phi} = \frac{\int d^3\mathbf{r}\Phi(\mathbf{r})n(\mathbf{r})}{\int d^3\mathbf{r}n(\mathbf{r})}. \quad (1)$$

Here, $n(\mathbf{r})$ is the electron density of either the isolated 5A1 or the isolated 5A2 molecule with their positions and geometries taken from the full 5A/Cs/Ag DFT calculations. Thus, Eq. (1) describes an average of the electrostatic potential weighted by the charge density distribution $n(\mathbf{r})$ of the molecule. Thereby, we obtain values of $\bar{\Phi}_{5A1} = -0.30$ eV and $\bar{\Phi}_{5A2} = +0.82$ eV for model I, and a common value of $\bar{\Phi}_{5A1} = \bar{\Phi}_{5A2} = +0.26$ eV for model II with respect to the calculated average work function of the Cs-doped Ag(110) surface. Note that we have also indicated these average potential values by coloring the respective molecules according to the color map shown in panels (b) and (d). These local differences on the potential are the driving force for the experimentally observed energy differences between the doped and hybridized 5A molecular states.

The measured work functions in the first doping regime can be considered to be the average of the local work functions at the regions of hybridized (Φ_1) and doped molecules (Φ_2)

$$\Phi(x) = x\Phi_1 + (1-x)\Phi_2, \quad (2)$$

where x is the surface area of doped molecules normalized to 1. The values of the local work functions can be taken from the completely hybridized monolayer ($\Phi_1 = 3.9$ eV) and the completely doped monolayer ($\Phi_2 = 2.7$ eV). The values of x have been derived in two ways, first from relative emission intensities of the doped LUMO assuming completed doping at $\Theta_{Cs} = 0.14$, and second from the Cs exposure assuming completed monolayer doping ($x = 1$) at $\Theta_{Cs} = 0.14$. As plotted in Fig. 3, both yield average work function values in striking agreement with measured work functions. This supports (i) the simple argument of the work function being the area average of local work functions, (ii) the local work function at doped 5A molecules indeed being 2.7 eV, and (iii) completed monolayer doping takes place at $\Theta_{Cs} = 0.14$ (2Cs per molecule). As a more general conclusion, our analysis also indicates that ARUPS can indeed provide quantitative information on the composition of multicomponent systems provided that the photoemission distribution has been understood and experimental geometry chosen appropriately.

2. *Second dosing regime: Continuous level shifts*

It is proposed that, for exposures beyond $\Theta_{Cs} = 0.14$, the excess Cs goes to the Ag surface. This is evidenced by the appearance of an emission at 11.6 eV (see Fig. 2), corresponding to the energy of $Cs_{5p3/2}$ emission of Cs on the clean Ag. This Cs/Ag emission´s binding energy is independent of the Cs coverage, and it only appears once doping is completed. This is in contrast to the second Cs peak (Cs/5A), which up to completion of monolayer doping, is observed at a binding energy of 12.1 eV, but once doping is completed, shifts towards higher binding energy with decreasing work function in the same way as the molecular features. Therefore, we attribute this $Cs_{5p3/2}$ emission to Cs in the charge transfer molecular complex (Cs/5A). The continuous shift of the binding energies of molecular emissions in the second regime as a function of the average work function suggests that, beyond complete monolayer doping, the excess Cs lifts the doped monolayer from the surface [38]. The calculations of the electrostatic potential of Fig. 4 indicate that, around 4 Å above the surface, the molecules will effectively feel an average potential.

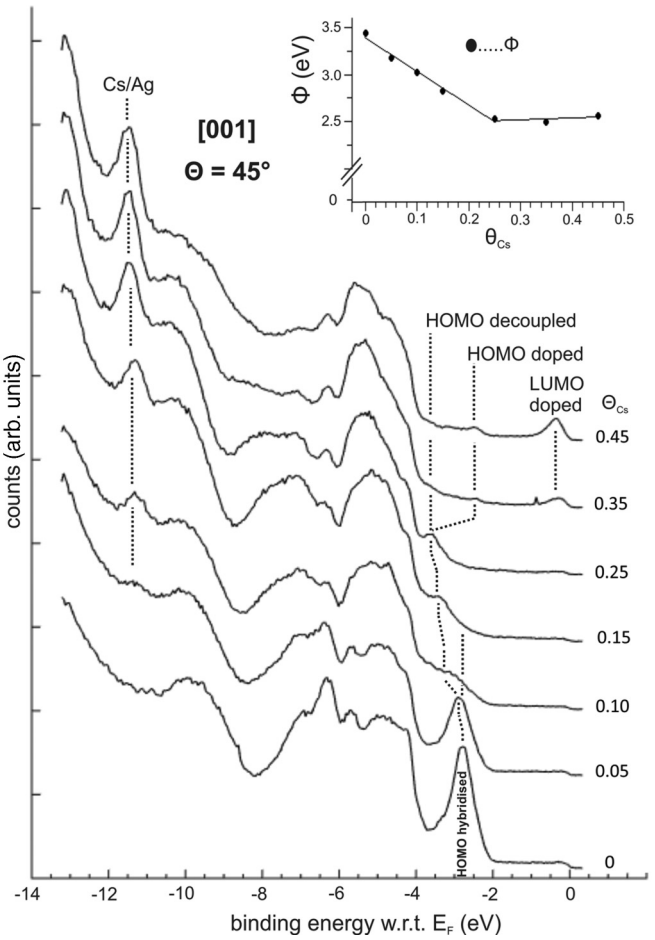

FIG. 6. He I ARUPS of a 6P monolayer on Ag(110) with subsequent Cs deposition in the [001] azimuth at 45° takeoff angle. Cs coverages are indicated to the right of the spectra. Diagram on top displays the work function behavior of the 6P monolayer on Ag(110) on Cs exposure.

3. Summary

A summary of the observed energy level alignments of a 5A monolayer on Ag(110) during the doping process is given in Fig. 5. Additionally, a schematic showing the orientation of molecules on the surface is displayed, with no intention of inferring domain sizes. The orientation and character of the molecules on the surface is color coded: black indicates hybridized molecules oriented along [001], while red denotes doped molecules oriented in [1$\bar{1}$0]. The background color reflects the local work functions. Light blue is the hybridized case, and light brown is the work function at doped 5A. Column one displays the 5A monolayer on Ag(110) without Cs, where all molecules align to the same work function. Column two illustrates the intermediate stage, where doped and hybridized molecules coexist. The two molecular species align to the respective characteristic work functions of 3.9 eV (hybridized) and 2.7 eV (doped). Note that, on enhanced screening and possible stabilization effects, the IP of doped 5A is reduced compared to the hybridized case. At a Cs exposure of $\Theta_{Cs} = 0.14$ (column three), all molecules are doped, revealing a uniform energy level alignment. On even higher Cs exposures, a continuous energy level alignment is observed when increasing the Cs exposure due to the lifting of doped molecules from the substrate surface and alignment to the average potential further away from the surface.

We take a closer look at the Cs exposure required to advance from completed doping to the saturation at the interface in order to shed light on the LUMO occupancy upon doping. Saturation takes place at a Cs coverage of 0.36, while completed doping is accomplished at $\Theta_{Cs} = 0.14$. This implies that an excess of $\Theta_{Cs} = 0.22$ can be added. This is roughly the amount of Cs that can be adsorbed on the Ag(110) surface at room temperature ($\Theta_{Cs} = 0.25$). This suggests that the excess Cs indeed forms an (ionic) decoupling Cs/Ag layer lifting the

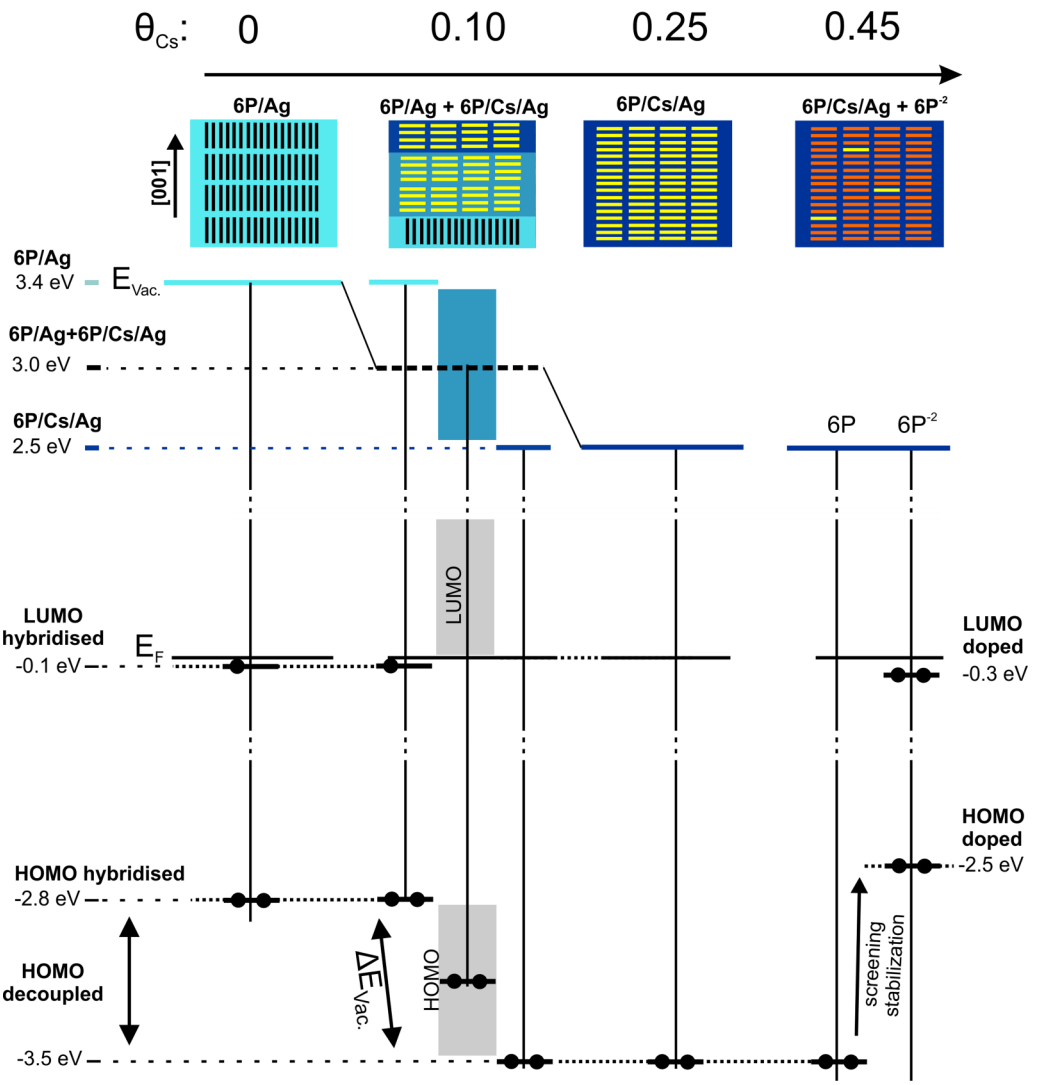

FIG. 7. Schematic of the energy level alignment for a hybridized 6P monolayer on Ag(110) on Cs doping. The first column illustrates the energy level alignment for the undoped monolayer. The broad lines at a Cs coverage of 0.10 reflect the various local work functions (energy level alignments) due to inhomogeneous Cs densities in the vicinity of molecules. Column 3 shows the situation at completed monolayer decoupling, $\Theta_{Cs} = 0.25$. The situation on additional Cs exposure ($\Theta_{Cs} = 0.45$), close to completed monolayer doping, is displayed in Column 4.

doped 5A layer with two Cs atoms per charge complex from the surface. While located directly at the Ag surface, it is not clear what the degree of charge transferred to the molecule will be. For the decoupled charge transfer complex, one electron per Cs can be expected. This implies full 5A LUMO occupancy with two electrons transferred from the Cs atoms to the molecule.

The question now addressed is why only doubly charged $5A^{-2}$ (two Cs) is observed and never the singly doped $5A^{-1}$ (one Cs). Only an integer number of Cs atoms can be expected to alter the electrostatic potential at a molecule due to its very limited spatial extent relative to the rather delocalized molecular electronic structure. To understand the exclusion of charge transfer complexes involving only one Cs atom, the Cs-induced potential changes must be considered. The local work function at doped 5A, containing two Cs atoms, is 2.7 eV, with the LUMO observed 0.5 eV below the Fermi level. The removal of one Cs atom would raise the potential by 0.6 (simulation), consequently positioning the LUMO 0.1 eV above E_F, which would thus be empty with the consequence of no $5A^{-1}$ charge transfer complex formation [39].

B. 6P on Cs exposure

In order to further test these arguments relying on the local character of the work function changes upon doping, we now turn to a different molecule, 6P, which is almost twice as long as 5A and exhibits a somewhat smaller EA compared to 5A. The comparison is cogent as the frontier orbitals of both are delocalized π orbitals; moreover, both molecules bond similarly to the Ag(110) substrate (flat lying across the atomic rows with the LUMOs partially occupied at the Fermi level), and ultimately both form charge transfer salts with Cs. The general behavior of the 6P monolayer on Ag(110) on Cs exposure is similar to that reported for the 6P monolayer on Cu(110) [12]. Unlike the case for the 5A monolayer, Cs first decouples all the 6P molecules in the monolayer from the substrate before doping can proceed. The initial exposure regime up to the point where doping becomes significant is displayed in Fig. 6. The spectra have been recorded along the [001] azimuth at a takeoff angle of 45°, where the hybridized HOMO is visible, and on reorientation to the [1$\bar{1}$0] azimuth, the doped LUMO should appear.

Up to an exposure of $\Theta_{Cs} = 0.25$, all molecular emissions shift quasicontinuously to higher binding energies with decreasing work function. The very intense hybridized HOMO peak at 2.7 eV all but disappears by $\Theta_{Cs} = 0.10$, and by $\Theta_{Cs} = 0.25$, the HOMO emissions of decoupled and undoped 6P can be found at 3.5 eV. Note, even at this relatively high Cs exposure, $\Theta_{Cs} \geqslant$ four Cs per 6P molecule (twice of that leading to complete doping of the 5A monolayer), there is no evidence for LUMO occupation, and also the $Cs_{5p3/2}$ emissions at 11.5 eV indicate Cs on Ag rather than in the molecular complex. For higher Cs exposures ($\Theta_{Cs} > 0.25$), doping begins with the LUMO appearing at 0.25 eV binding energy. On LUMO occupation, the HOMO of doped 6P is found at a lower binding energy due to enhanced screening and stabilization effects for $6P^{-2}$ compared to the neutral molecule [12]. The LUMO is fully occupied at $\Theta_{Cs} = 0.45$, which is equivalent to an exposure of seven Cs atoms per 6P molecule. The work function behavior on Cs exposure is summarized in the inset of Fig. 6. We observe the known 6P Cs-doping characteristic revealing an initial work function reduction on Cs exposure followed by a constant work function once doping begins [12].

A summary of the observed energy level alignment of a 6P monolayer on Ag(110) for the four characteristic stages up to doping is shown in the schematic of Fig. 7. The orientation of the molecules on the surface is indicated with the color of the molecule indicating its state: black reflects the hybridized case, yellow decoupled, and red doped. The background color reflects the local work functions. Light blue is the hybridized case, and dark blue is the work function at the maximum Cs exposure ($\Theta_{Cs} = 0.25$) prior to doping. At moderate Cs exposures ($\Theta < 0.25$), one observes decoupled molecules that experience work functions between hybridized (3.4 eV) and decoupled (2.5 eV) 6P. This leads to broad molecular emissions.

VI. CONCLUSION

Our data show that, for 5A, even the lowest Cs exposure leads to charge transfer doping, while in the case of 6P, doping only occurs at high Cs exposures after the complete monolayer is decoupled from the substrate. This different behavior observed for 5A and 6P can be understood when considering their different EAs and molecular dimensions. Compared to 5A, 6P is both larger (118 Å^2 versus 80 Å^2) and also has a lower EA (2.5 eV [40] versus 3.1 eV [40]). Charge transfer doping will occur when the LUMO is shifted below E_F, due to the Cs lowering the electrostatic potential in the region of the molecule below the molecule´s EA. The average electrostatic potential that a molecule experiences, however, is dependent on the size of the molecule relative to the spatial extent of the dopant's electrostatic potential. The larger the molecule, the lower the effect of the dopant's potential, and a greater number of dopants will be required to achieve charge transfer doping. This is exemplified by 6P here, where a large number (∼7) of dopants are required for doping to occur with quasicontinuous shift in level alignment up to this point. This leads to the observed complete decoupling of the whole monolayer prior to doping. For relatively small molecules and/or molecules with high EA, such as 5A in this paper, charge transfer can occur at the lowest doping level, leading to an interface containing a mixture of doped and adsorbed molecules. Then only after complete doping of the monolayer can a continuous shift of the level alignment with increasing dopant concentration occur.

ACKNOWLEDGMENTS

This paper has been financially supported by the Austrian Science Fund (FWF), Project Nos. P27427-N20 and P27649-N20. We thank HZB for the allocation of synchrotron radiation beam time. The research leading to these results has received funding from the European Community's Seventh Framework Programme (FP7/2007-2013) under Grant Agreement No. 226716. The computational results presented have been achieved using the Vienna Scientific Cluster (VSC).

[1] H. Ishii, K. Sugiyama, E. Ito, and K. Seki, Energy level alignment and interfacial electronic structures at organic metal and organic interfaces, Adv. Mater. **11**, 605 (1999).

[2] N. Koch, Organic electronic devices and their functional interfaces, Chem. Phys. Chem. **8**, 1438 (2007).

[3] Y. Shen, A. R. Hosseini, M. H. Wong, and G. G. Malliaras, How to make ohmic contacts to organic semiconductors, Chem. Phys. Chem. **5**, 16 (2004).

[4] V. I. Arkhipov, E. V. Emelianova, Y. H. Tak, and H. Bässler, Charge injection into light-emitting diodes: Theory and experiment, J. Appl. Phys. **84**, 848 (1998).

[5] S. Braun, W. R. Salaneck, and M. Fahlman, Energy-level alignment at organic/metal and organic/organic interfaces, Adv. Mater. **21**, 1450 (2009).

[6] J. B. Neaton, M. S. Hybertsen, and S. G. Louie, Renormalization of Molecular Electronic Levels at Metal-Molecule Interfaces, Phys. Rev. Lett. **97**, 216405 (2006).

[7] M. Willenbockel, D. Lüftner, B. Stadtmüller, G. Koller, C. Kumpf, S. Soubatch, P. Puschnig, M. G. Ramsey, and F. S. Tautz, The interplay between interface structure, energy level alignment and chemical bonding strength at organic-metal interfaces, Phys. Chem. Chem. Phys. **17**, 1530 (2015).

[8] M. G. Betti, F. Crispoldi, A. Ruocco, and C. Mariani, Insulating state of electron-doped Cu-phthalocyanine layers, Phys. Rev. B **76**, 125407 (2007).

[9] F. Bussolotti, S. Kera, and N. Ueno, Potassium doping of single crystalline pentacene thin film, Phys. Rev. B **86**, 155120 (2012).

[10] W. Gao and A. Kahn, Electrical doping: The impact on interfaces of π -conjugated molecular films, J. Phys. Condens. Matter **15**, S2757 (2003).

[11] S. Winkler, J. Frisch, R. Schlesinger, M. Oehzelt, R. Rieger, J. Räder, J. P. Rabe, K. Müllen, and N. Koch, The impact of local work function variations on Fermi level pinning of organic semiconductors, J. Phys. Chem. C **117**, 22285 (2013).

[12] E. M. Reinisch, T. Ules, P. Puschnig, S. Berkebile, M. Ostler, T. Seyller, M. G. Ramsey, and G. Koller, Development and character of gap states on alkali doping of molecular films, New J. Phys. **16**, 023011 (2014).

[13] X.-C. Guo and R. J. Madix, Adsorption of oxygen and carbon dioxide on cesium-reconstructed Ag(110) surface, Surf. Sci. **550**, 81 (2004).

[14] B. E. Haydn, K. C. Prince, P. J. Davie, G. Paolucci, and A. M. Bradshaw, Alkali metal induced reconstruction of Ag(110), Solid State Commun. **48**, 325 (1983).

[15] R. Döhl-Oelze, E. M. Stuve, and J. K. Sass, Thermal activation of the cesium induced reconstruction of Ag(110), Solid State Commun. **57**, 323 (1986).

[16] G. Koller, S. Berkebile, M. Oehzelt, P. Puschnig, C. Ambrosch-Draxl, F. P. Netzer, and M. G. Ramsey, Intra- and intermolecular band dispersion in an organic crystal, Science **317**, 351 (2007).

[17] S. Berkebile, G. Koller, A. Fleming, P. Puschnig, C. Ambrosch-Draxl, K. Emtsev, T. Seyller, J. Riley, and M. G. Ramsey, The electronic structure of pentacene revisited, J. Electron Spectros. Relat. Phenomena **174**, 22 (2009).

[18] H. Kakuta, T. Hirahara, I. Matsuda, T. Nagao, S. Hasegawa, N. Ueno, and K. Sakamoto, Electronic Structures of the Highest Occupied Molecular Orbital Bands of a Pentacene Ultrathin Film, Phys. Rev. Lett. **98**, 247601 (2007).

[19] N. Jiri, M. Oehzelt, S. Berkebile, M. Koini, T. Ules, G. Koller, T. Haber, and M. G. Ramsey, Crystal growth of para-sexiphenyl on clean and oxygen reconstructed Cu(110) surfaces, Phys. Chem. Chem. Phys **13**, 14675 (2011).

[20] P. Puschnig, S. Berkebile, A. Fleming, G. Koller, K. Emtsev, T. Seyller, J. D. Riley, C. Ambrosch-Draxl, F. P. Netzer, and M. G. Ramsey, Reconstruction of molecular orbital densities from photoemission data, Science **326**, 702 (2009).

[21] P. Puschnig, E. M. Reinisch, T. Ules, G. Koller, S. Soubatch, M. Ostler, L. Romaner, F. S. Tautz, and M. G. Ramsey, Orbital tomography: Deconvoluting photoemission spectra of organic molecules, Phys. Rev. B **84**, 235427 (2011).

[22] M. Wießner and N. S. Rodr, Different views on the electronic structure of nanoscale graphene: Aromatic molecule versus quantum dot, New J. Phys. **14**, 113008 (2012).

[23] D. Lüftner, M. Milko, S. Huppmann, M. Scholz, N. Ngyuen, M. Wießner, A. Schöll, F. Reinert, and P. Puschnig, CuPc/Au(110): Determination of the azimuthal alignment by a combination of angle-resolved photoemission and density functional theory, J. Electron Spectros. Relat. Phenomena **195**, 293 (2014).

[24] M. Willenbockel, B. Stadtmüller, K. Schönauer, F. C. Bocquet,, D. Lüftner, E. M. Reinisch, T. Ules, G. Koller, C. Kumpf, S. Soubatch, P. Puschnig, M. G. Ramsey, and F. S. Tautz, Energy offsets within a molecular monolayer: The influence of the molecular environment, New J. Phys. **15**, 033017 (2013).

[25] M. Wießner, D. Hauschild, A. Schöll, F. Reinert, V. Feyer, K. Winkler, and K. Krömker, Electronic and geometric structure of the PTCDA/Ag(110) interface probed by angle-resolved photoemission, Phys. Rev. B **86**, 045417 (2012).

[26] E. M. Reinisch, P. Puschnig, T. Ules, M. G. Ramsey, and G. Koller, Layer resolved photoemission tomography: The p-sexiphenyl bilayer upon Cs doping, Phys. Rev. B **93**, 155438 (2016).

[27] T. Ules, D. Lüftner, E. M. Reinisch, G. Koller, P. Puschnig, and M. G. Ramsey, Orbital tomography of hybridized and dispersing molecular overlayers, Phys. Rev. B **90**, 155430 (2014).

[28] L. Broekman, A. Tadich, E. Huwald, J. Riley, R. Leckey, T. Seyller, K. Emtsev, and L. Ley, First results from a second generation toroidal electron spectrometer, J. Electron Spectros. Relat. Phenomena **144–147**, 1001 (2005).

[29] G. Kresse and J. Hafner, *Ab initio* molecular dynamics for liquid metals, Phys. Rev. B **47**, 558 (1993).

[30] G. Kresse and D. Joubert, From ultrasoft pseudopotentials to the projector augmented-wave method, Phys. Rev. B **59**, 1758 (1999).

[31] J. Neugebauer and M. Scheffler, Adsorbate-substrate and adsorbate-adsorbate interactions of Na and K adlayers on Al(111), Phys. Rev. B **46**, 16067 (1992).

[32] J. P. Perdew, K. Burke, and M. Ernzerhof, Generalized Gradient Approximation Made Simple, Phys. Rev. Lett. **77**, 3865 (1996).

[33] P. E. Blöchl, Projector augmented-wave method, Phys. Rev. B **50**, 17953 (1994).

[34] S. Grimme, J. Antony, S. Ehrlich, and H. Krieg, A consistent and accurate *ab initio* parametrization of density functional dispersion correction (DFT-D) for the 94 elements H-Pu, J. Chem. Phys. **132**, 154104 (2010).

[35] D. Lüftner, T. Ules, E. M. Reinisch,, G. Koller, S. Soubatch, F. S. Tautz,, M. G. Ramsey, and P. Puschnig, Imaging the wave functions of adsorbed molecules, Proc. Natl. Acad. Sci. USA **111**, 605 (2014).

[36] S. Berkebile, P. Puschnig, G. Koller, M. Oehzelt, F. Netzer, C. Ambrosch-Draxl, and M. G. Ramsey, Electronic band structure

of pentacene: An experimental and theoretical study, Phys. Rev. B **77**, 115312 (2008).

[37] T. Ules, Ph.D. thesis, Orbital tomographic investigations of organic molecular films and their interfaces, Karl-Franzens University Graz, 2014.

[38] G. Koller, B. Winter, M. Oehzelt, J. Ivanco, F. P. Netzer, and M. G. Ramsey, The electronic band alignment on nanoscopically patterned substrates, Org. Electron. **8**, 63 (2007).

[39] O. T. Hofmann, P. Rinke, M. Scheffler, and G. Heimel, Integer versus fractional charge transfer at metal (/insulator)/organic interfaces: Cu (/NaCl)/TCNE, ACS Nano **9**, 5391 (2015).

[40] P. Puschnig and D. Lüftner, Simulation of angle-resolved photoemission spectra by approximating the final state by a plane wave: From graphene to polycyclic aromatic hydrocarbon molecules, J. Electron Spectros. Relat. Phenomena **200**, 193 (2015).